Supplement of The Cryosphere, 17, 2095–2118, 2023
https://doi.org/10.5194/tc-17-2095-2023-supplement

The Cryosphere
Open Access

Supplement of

Representation of soil hydrology in permafrost regions may explain large part of inter-model spread in simulated Arctic and subarctic climate

Philipp de Vrese et al.

Correspondence to: Philipp de Vrese (philipp.de-vrese@mpimet.mpg.de)

S1 Soil hydrology in PCN-MIP participants

Many factors that are especially relevant for permafrost-affected areas are treated very differently by current-generation land surface models. Here, one prominent example is the process of supercooling which is included in roughly half of the models participating in the PCN-MIP[1]. In clay rich soils a substantial fraction of water may remain liquid at sub-zero temperatures and potentially move through and drain from the soil even if the model considers the effect of soil ice on the hydraulic conductivity – which many models do using a power-law-based ice impedance factor. Another, important factor is the treatment of soil organic matter, which is also explicitly included in about half of the PCN-MIP participants. Here, the importance of a high soil organic matter concentration is often attributed to its impact on the soil thermal properties, as the high porosity can provide a strong insulation at the surface of dry soils. However, soil organic matter also affects the hydrological properties, increasing conductivity, hence, the percolation into deeper layers and drainage. This affects the water available for transpiration and evaporation, with a strong impact on the surface energy budget.

At the same time, most present-day land surface models use similar formulations to represent some of the key processes of the terrestrial hydrology[1,2]. For example, the majority of models employs a 1-D formulation based on the Richards equations with Clapp–Hornberger or van Genuchten functions to describe the vertical movement of water through the soil, while surface runoff and infiltration are most often described using a saturation-excess based formulation. But while these approaches appear similar, they may yield diverging results, depending on the specifics of their implementation. For example, the infiltration in a saturation-excess based formulation depends on the way the model determines the surbgrid scale distribution of the water table or, if the model instead uses the soil field capacity or porosity as an upper limit for infiltration, on the assumption up to which soil layer water can infiltrate within one timestep. The same is true for the representation of evapotranspiration as most models account for the same sources but employ different formulations to describe the respective fluxes.

It is exceedingly difficult to quantify how a given parametrization affects the modelling outcome as it is very often the interactions between processes that determine the behaviour of a given model. This is particularly problematic as differences in the simulated soil hydrology may also originate from differences in the treatment of the soil thermal dynamics – as these determine the state of water in the soil – as well as from differences in the general model setup, e.g. vertical resolution and depth of the soil column, and the representation of vegetation. Thus, our JSBACH setups merely aim at capturing the bulk effects of the uncertainty included in the range of established soil hydrology representations without trying to connect them to specific formulations employed by present-day land surface models. A brief overview of the hydrology characteristics of the PCN-MIP participants is provided in table ST1, while a more detailed discussion can be found in Andresen et al. (2020)[1].

Model	Evapotranspiration	Runoff / Infiltration	Vertical transport	Ice impact on soil properties	Super-cooling	Organic matter
CLM 4.5	Canopy evaporation + transpiration + soil evaporation	Saturation-excess (f(wt[3]))	Richards equation (Clapp–Hornberger)	Power-law ice impedance[4]	Yes	Yes
CoLM	BATS[5] and Philip's[6]	Saturation-excess (f(wt)[7])	Richards equation (Clapp–Hornberger)	Power-law ice impedance	No	No
JULES	Transpiration + soil evaporation + moisture storages (e.g., lakes, urban) - surface resistance	Saturation-excess (f(wt[7]), f(θ))	Richards equation (Clapp–Hornberger, van Genuchten)	Implicit (Brooks and Corey)	Yes	No
ORCHIDEE-IPSL	Soil evaporation + interception loss + transpiration	Saturation-excess (f(θ))	Richards equation (van Genuchten)	"Drying = freezing" approximation[8]	Yes	Yes
LPJGUESS	Interception loss + transpiration + soil evaporation[9]	Depends on soil moisture and layer thickness, declines exponentially with soil moisture	Analog to Darcy'slaw[10]	Power-law ice impedance	No	No
SIBCASA	soil evaporation + surface dew + canopy ET + canopy dew[11]	Based on Darcy's law	Richards equation (Clapp–Hornberger)	Power-law ice impedance	Yes	Yes
TEM-604	Jensen–Haise potential ET[12]; actual ET is calculated based on PET, water availability and leaf mass	Saturation-excess (f(θ))[13]	One-layer bucket	None	No	No
UWVIC	Canopy interception + transpiration + soil evaporation[14]	Saturation-excess (f(θ))	Based on shape parameters[14]	Power-law ice impedance	Yes	Yes
JSBACH (standard)	Transpiration + soil evaporation + canopy evaporation + snow evaporation	ARNO - rainfall -runoff model[15]	Richards equation (van Genuchten)	None	No	No
JSBACH (WET)	Transpiration + soil evaporation + canopy evaporation + snow evaporation	ARNO model combined with WEED scheme[16] (F_{ARNO} = 1.0)	Richards equation (van Genuchten)	Power-law ice impedance; no movement if ice volume > 50% pore space	Yes	Yes
JSBACH (DRY)	Transpiration + soil evaporation + canopy evaporation + snow evaporation	ARNO model combined with WEED scheme[16] (F_{ARNO} = 0.8)	Richards equation(van Genuchten)	Power-law ice impedance	Yes	Yes

Supplementary Table ST1. Hydrology characteristics of land surface models participating in the PCN-MIP. Note that the table was adapted from Andresen et al. (2020)[1], with JSBACH not being part of the PCN-MIP.

S2 CMIP6 models included in the analysis

Models	Institution
ACCESS-ESM1.5; ACCESS-CM2[17,18]	Commonwealth Scientific and Industrial Research Organisation; Australian Research Council Centre of Excellence for Climate System Science (Australia)
AWI[19]	Alfred Wegener Institute, Helmholtz Centre for Polar and Marine Research (Germany)
BCC-CSM2-MR[20]	Beijing Climate Center (China)
CAMS-CSM1.0[21]	Chinese Academy of Meteorological Sciences (China)
CanESM5-CanOE; CanESM5[22]	Canadian Centre for Climate Modelling and Analysis (Canada)
CESM2-CAM6; CESM2-WACCM6[23]	National Center for Atmospheric Research (USA)
CIESM[24]	Department of Earth System Science, Tsinghua University (China)
CMCC-ESM2; CMCC-CM2-SR5[25]	Centro Euro-Mediterraneo sui Cambiamenti Climatici (Italy)
CNRM-CM6.1-HR; CNRM-CM6.1; CNRM-ESM2.1[26–28]	Centre National de Recherches Meteorologiques; Centre Europeen de Recherche et de Formation Avancee en Calcul Scientifique (France)
E3SM-1.1[29,30]	Department of Energy (USA)
EC-Earth3; EC-Earth3-Veg0; EC-Earth3-CC; EC-Earth3-Veg-LR[31]	EC-Earth consortium, Rossby Center, Swedish Meteorological and Hydrological Institute (Sweden)
FGOALS-f3-L; FGOALS-g3[32–34]	Institute of Atmospheric Physics (China)
FIO-ESM-2.0[35]	First Institute of Oceanography (China)
GFDL-CM4; GFDL-ESM4[36,37]	National Oceanic and Atmospheric Administration, Geophysical Fluid Dynamics Laboratory (USA)
GISS-E2.1-G[38,39]	Goddard Institute for Space Studies (USA)
IITM-ESM[40]	Centre for Climate Change Research, Indian Institute of Tropical Meteorology (India)
INM-CM5.0; INM-CM4.8[41,42]	Institute for Numerical Mathematic (Russia)
IPSL-CM6A-LR[43–45]	Institut Pierre-Simon Laplace (France)
K-ACE-1-0-G[46]	National Institute of Meteorological Sciences, Korea Meteorological Administration (South Korea)
KIOST-ESM[47]	Korea Institute of Ocean Science and Technology (Korea)
MIROC6; MIROC-ES2L[48,49]	Japan Agency for Marine-Earth Science and Technology; National Institute for Environmental Studies; Atmosphere and Ocean Research Institute, The University of Tokyo; RIKEN Center for Computational Science (Japan)
MPI-ESM1.2-LR; MPI-ESM1.2-HR[50,51]	Max Planck Institute for Meteorology; Deutsches Klimarechenzentrum; Deutscher Wetterdienst (Germany)
MRI-ESM2.0[52]	Meteorological Research Institute (Japan)
NESM3[53]	Nanjing University of Information Science and Technology (China)
NorESM2-LM; NorESM2-MM[54–56]	Norwegian Climate Center (Norway)
TaiESM[57]	Research Center for Environmental Changes, Academia Sinica (Taiwan)
UKESM1.0-LL; HadGEM3-GC31-LL; HadGEM3-GC31-MM[58–60]	Met Office Hadley Center; Natural Environment Research Council (UK)

Supplementary Table ST2. CMIP6 participants included in analysis

S3 Comparison to observations (MPI-ESM)

Var.	REF Bias (RMSE)	WET Bias (RMSE)	DRY Bias (RMSE)	W2D Bias (RMSE)	Source	Unit	Period	Fig.
$Temp_{2m}$	0.62 (3.16)	-0.85 (3.11)	1.94 (3.67)	**0.04** (2.78)	GSWP3	[K]	1990 - 2014	SF1
MAGT	-1.95 (3.9)	-2.49 (3.8)	**-0.17** (2.77)	-1.70 (3.44)	GTNP	[K]	2000 - 2010	SF2
$Thaw_{max}$	2.00 (2.30)	**0.08** (1.09)	1.39 (1.85)	0.27 (1.11)	CALM	[m]	1990 - 2019	SF3
Precip	8.42 (23.75)	7.24 (23.61)	**4.59** (21.34)	6.87 (22.97)	GSWP3	[mm mon^{-1}]	1990 - 2014	SF4
Snow	-16.46 (66.36)	**-12.67** (66.00)	-17.53 (66.78)	-15.18 (66.06)	CMC	[mm]	1998 - 2012	SF8
Discharge	295	275	**234**	279	GRDC	[km^3 yr^{-1}]	1980 - 1995	SF9
cf_{Tree}	-4.3 (22.98)	-13.40 (24.38)	**-1.05** (25.95)	-12.22 (23.74)	ESACCI	[%]	1992 - 2020	SF6
cf_{Grass}	24.48 (33.62)	25.42 (34.72)	**20.23** (27.96)	25.48 (33.60)	ESACCI	[%]	1992 - 2020	SF7
cf_{Shrub}	-5.58 (12.05)	-5.44 (10.14)	-7.01 (13.63)	**-4.71** (10.43)	ESACCI	[%]	1992 - 2020	SF8

Supplementary Table ST3. Overview over simulation biases in the northern permafrost regions for the different model setups, namely the reference model (REF), the WET setup, the DRY setup and the W2D setup. Given are the biases and root mean square errors for seasonally averaged 2m temperature relative to data from the Global Soil Wetness Project (GSWP3)[61,62], mean annual ground temperature (MAGT) relative to data from the Global Terrestrial Network for Permafrost (GTNP)[63–65], maximum annual thaw depths relative to data from Circumpolar Active Layer Monitoring (CALM)[66], mean seasonal precipitation relative to GSWP3 data, annual mean snow water equivalent relative to data from the Northern Hemisphere subset of the Canadian Meteorological Centre (CMC) operational global daily snow depth analysis[67], annual river discharge of the 5 largest Arctic rivers relative to data from the Global Runoff Data Centre (GRDC)[68] and tree-, grass- and shrub cover fractions relative to ESA Climate Change Initiative (ESACCI) data[69]. Bold numbers indicate the simulation exhibiting the smallest bias.

Var.	REF Bias (RMSE)	WET Bias (RMSE)	DRY Bias (RMSE)	W2D Bias (RMSE)	Source	Unit	Period	Fig.
$Temp_{2m}$	-0.60 (2.85)	-0.90 (2.93)	**-0.16** (2.68)	-0.65 (2.94)	GSWP3	[K]	1990 - 2014	SF1
Precip	**-1.39** (40.59)	-1.65 (40.18)	-1.49 (40.89)	-1.59 (39.54)	GSWP3	[mm mon^{-1}]	1990 - 2014	SF4
cf_{Tree}	4.73 (22.21)	**1.97** (22.71)	5.23 (23.29)	2.06 (22.36)	ESACCI	[%]	1992 - 2020	SF6
cf_{Grass}	17.55 (27.1)	17.56 (27.34)	**17.03** (25.60)	17.97 (27.18)	ESACCI	[%]	1992 - 2020	SF7
cf_{Shrub}	-8.78 (15.28)	-8.74 (14.83)	-9.15 (15.74)	**-8.46** (14.90)	ESACCI	[%]	1992 - 2020	SF8

Supplementary Table ST4. Overview over simulation biases across all continental areas for the different model setups, namely the reference model (REF), the WET setup, the DRY setup and the W2D setup. Given are the biases and root mean square errors for seasonally averaged 2m temperature relative to data from the Global Soil Wetness Project (GSWP3)[61,62], mean seasonal precipitation relative to GSWP3 data and tree-, grass- and shrub cover fractions relative to ESA Climate Change Initiative (ESACCI) data[69]. Bold numbers indicate the simulation exhibiting the smallest bias.

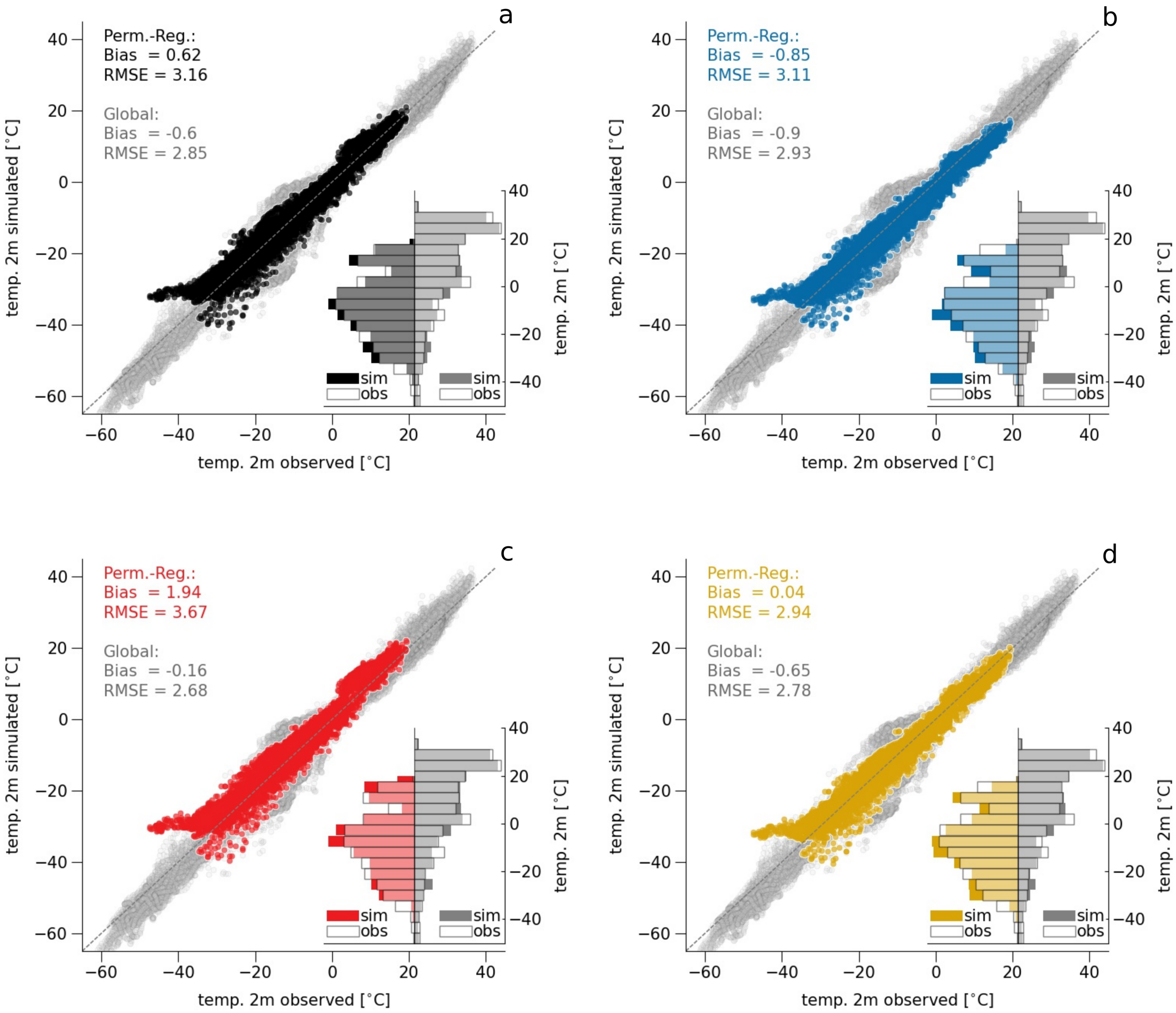

Supplementary Figure SF1. **2m temperature**
Comparison of simulated and observation based (Global Soil Wetness Project (GSWP3)[61,62]) seasonally averaged 2m temperature for: a) MPI-ESM1.2 standard version (black), b) WET setup (blue), c) DRY setup (red) and d) W2D setup (yellow). The data is averaged over the period 1990 - 2014. In the main panel each dot represents one season and one grid-box, with the colored dots referring to the northern permafrost regions, while grey dots refer to all continental areas. The same color-coding is valid in the histogram on the bottom right.

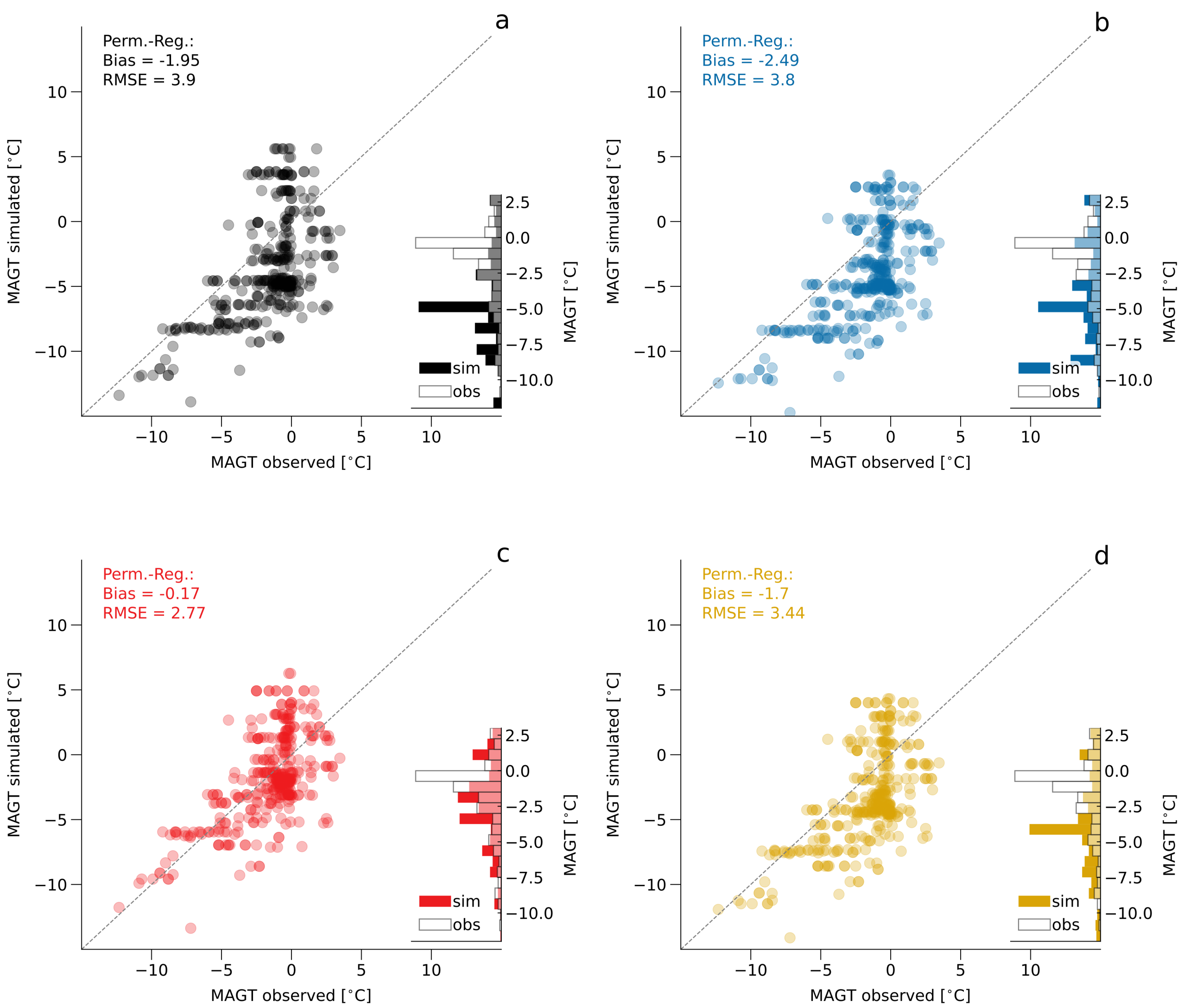

Supplementary Figure SF2. Mean annual ground temperature
Comparison of simulated and observed (Global Terrestrial Network for Permafrost (GTNP)[63–65]) mean annual ground temperatures (MAGT) in the northern permafrost regions for: a) MPI-ESM1.2 standard version (black), b) WET setup (blue), c) DRY setup (red) and d) W2D setup (yellow). For each site, the data is averaged over the period with available data between the years 2000 - 2010.

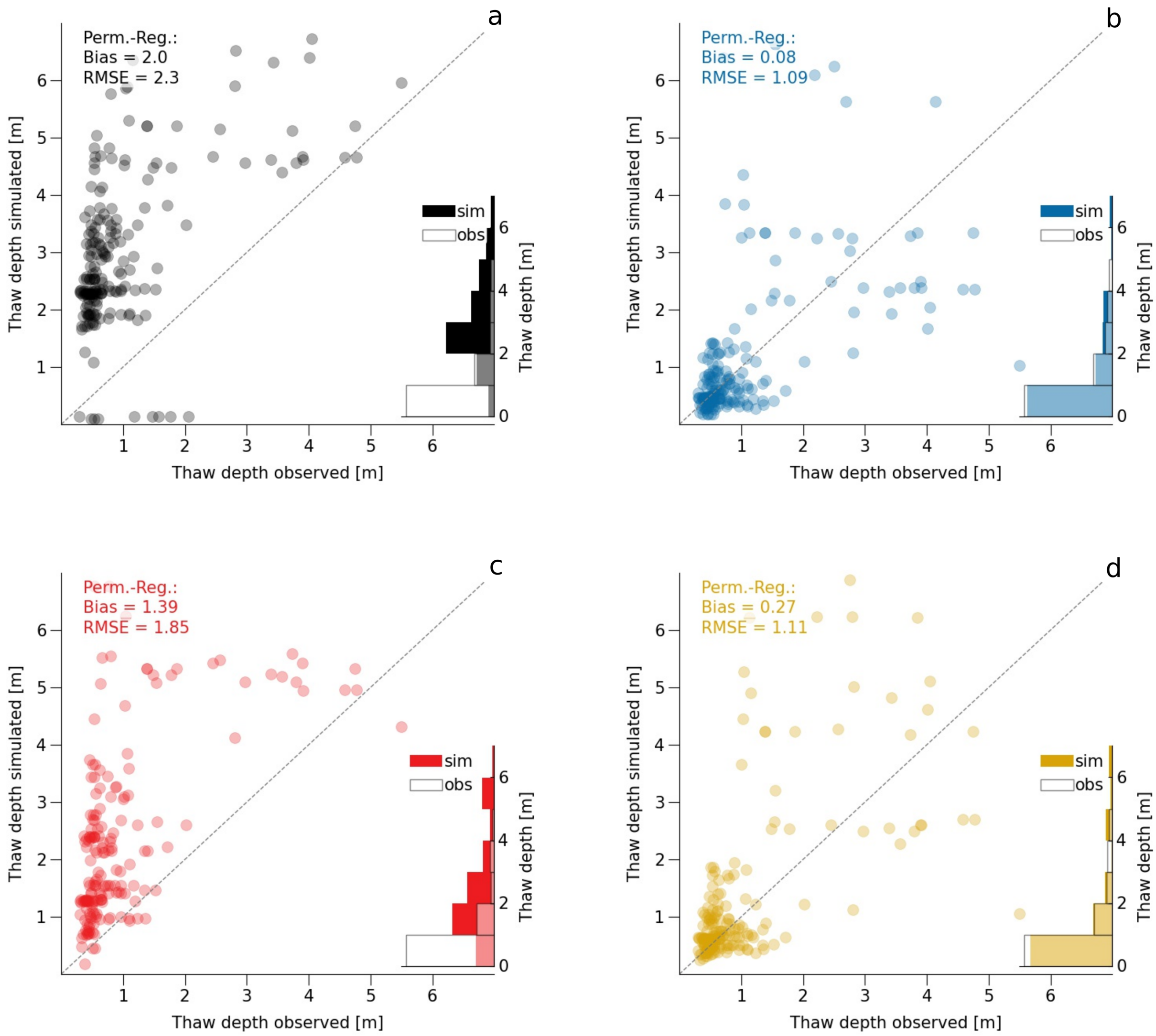

Supplementary Figure SF3. Maximum annual thaw depth
Comparison of simulated maximum annual thaw depths and observed end-of-season thaw depths (Circumpolar Active Layer Monitoring (CALM)[66]) in the northern permafrost regions for: a) MPI-ESM1.2 standard version (black), b) WET setup (blue), c) DRY setup (red) and d) W2D setup (yellow). For each site, the data is averaged over the period with available data between the years 1990 - 2019.

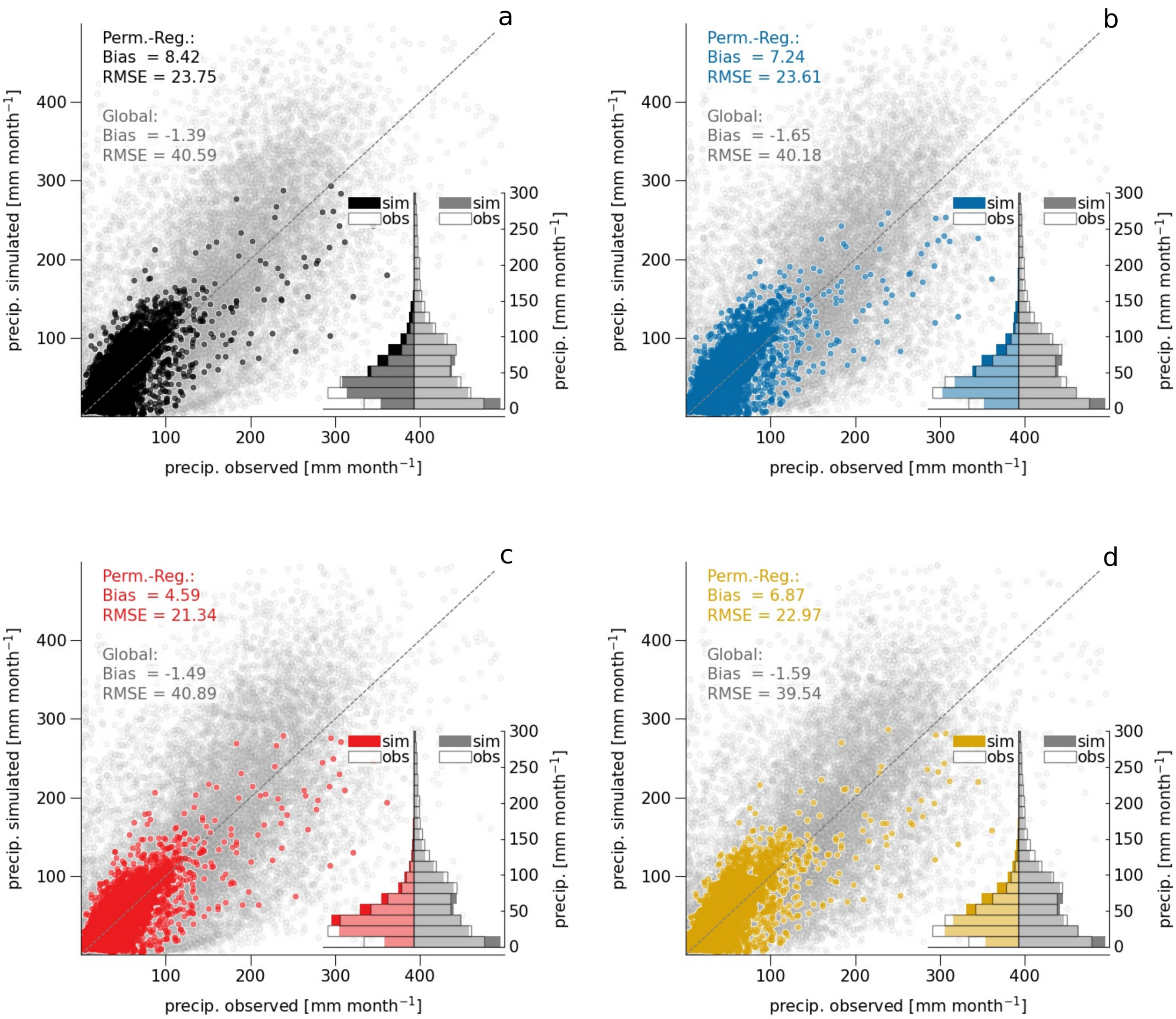

Supplementary Figure SF4. Precipitation

Comparison of simulated and observation based (Global Soil Wetness Project (GSWP3)[61,62]) seasonally averaged precipitation for: a) MPI-ESM1.2 standard version (black), b) WET setup (blue), c) DRY setup (red) and d) W2D setup (yellow). The data is averaged over the period 1990 - 2014.

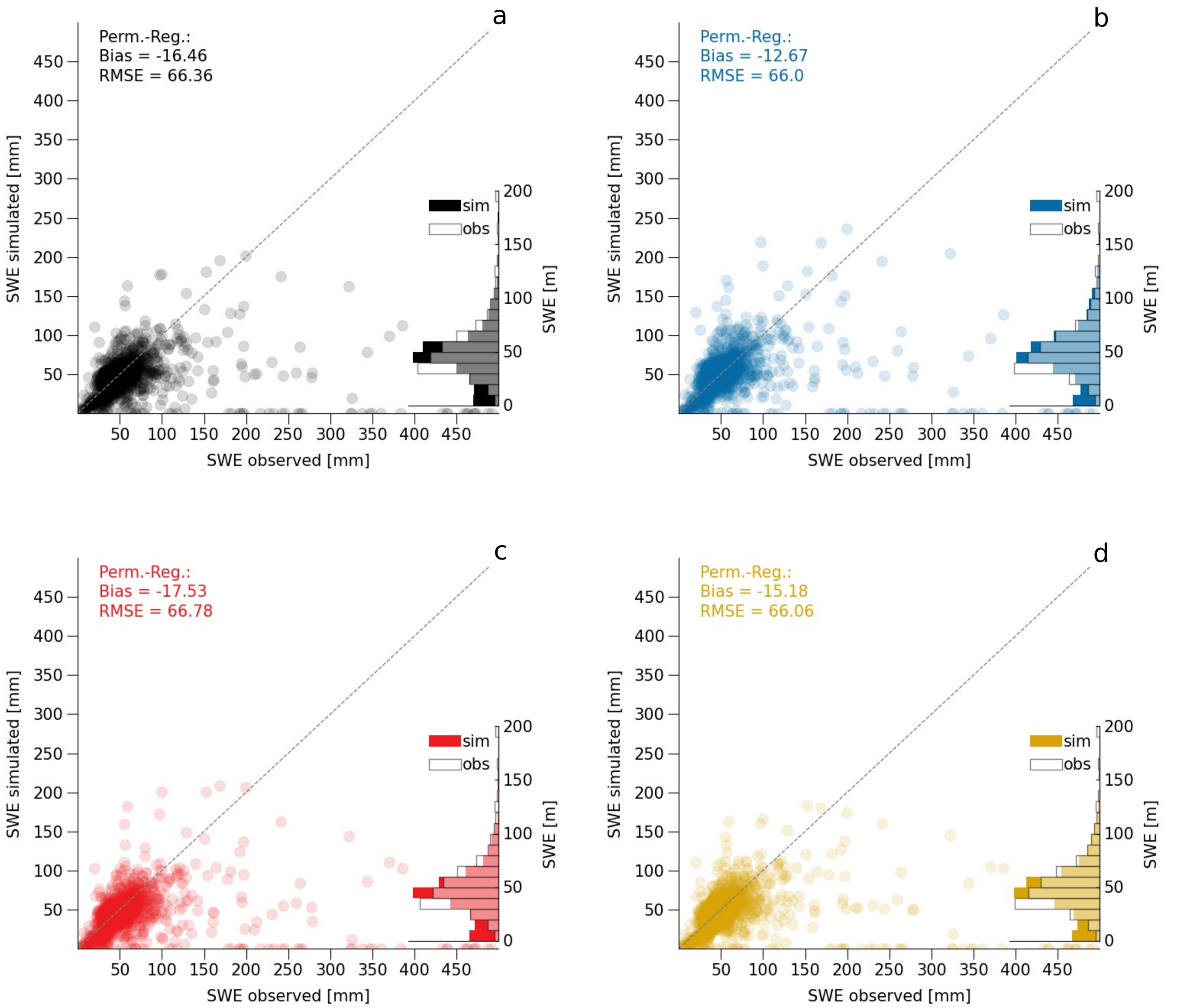

Supplementary Figure SF5. **Snow water equivalent**
Comparison of simulated and observed (Northern Hemisphere subset of the Canadian Meteorological Centre (CMC) operational global daily snow depth analysis[67]) annual average snow water equivalent in the northern permafrost regions for: a) MPI-ESM1.2 standard version (black), b) WET setup (blue), c) DRY setup (red) and d) W2D setup (yellow). The data is averaged over the period 1998 - 2012.

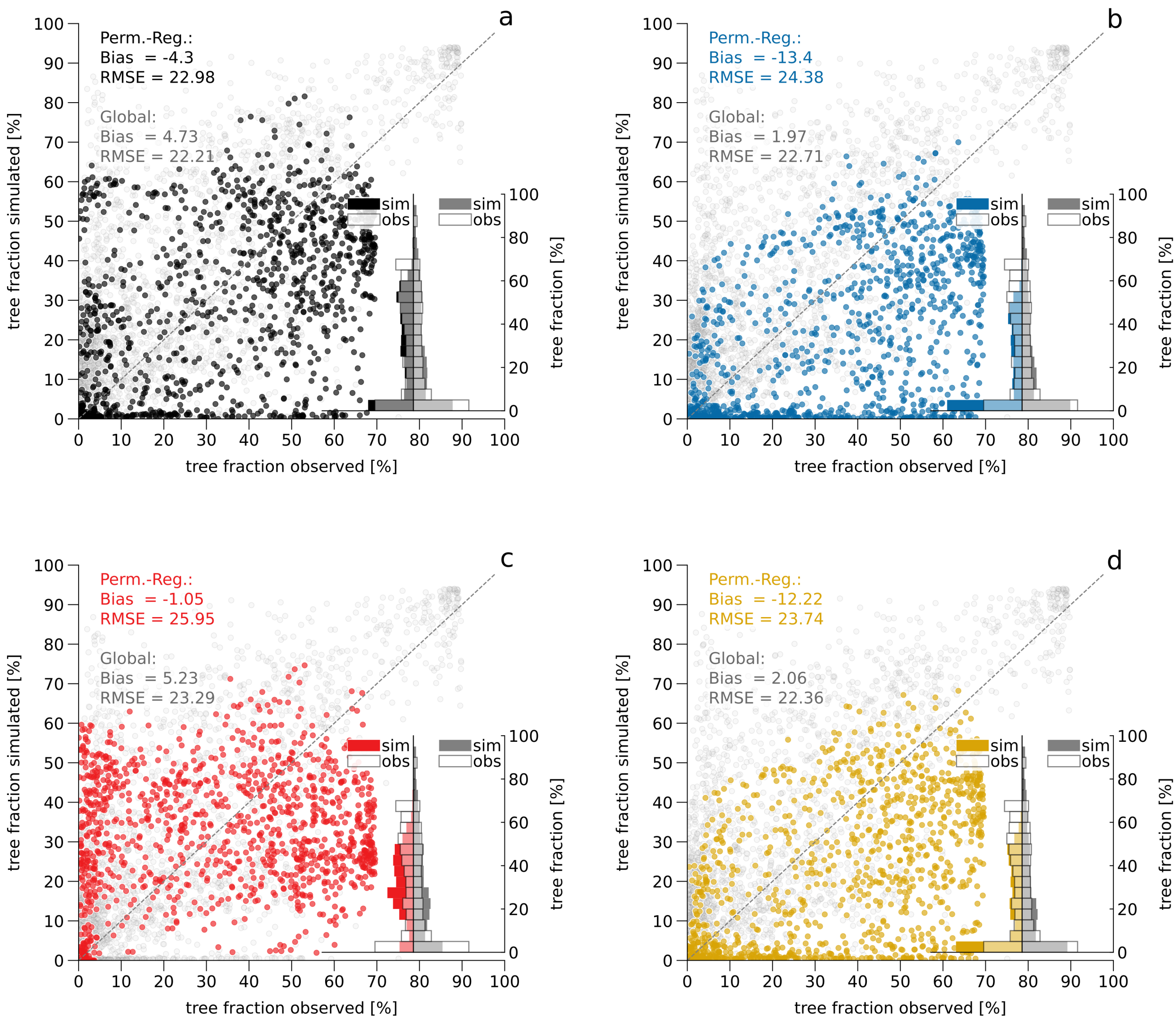

Supplementary Figure SF6. **Tree cover fraction**

Comparison of simulated and observed (ESA Climate Change Initiative (ESACCI)[69]) average tree cover for: a) MPI-ESM1.2 standard version (black), b) WET setup (blue), c) DRY setup (red) and d) W2D setup (yellow). The data is averaged over the period 1992 - 2020.

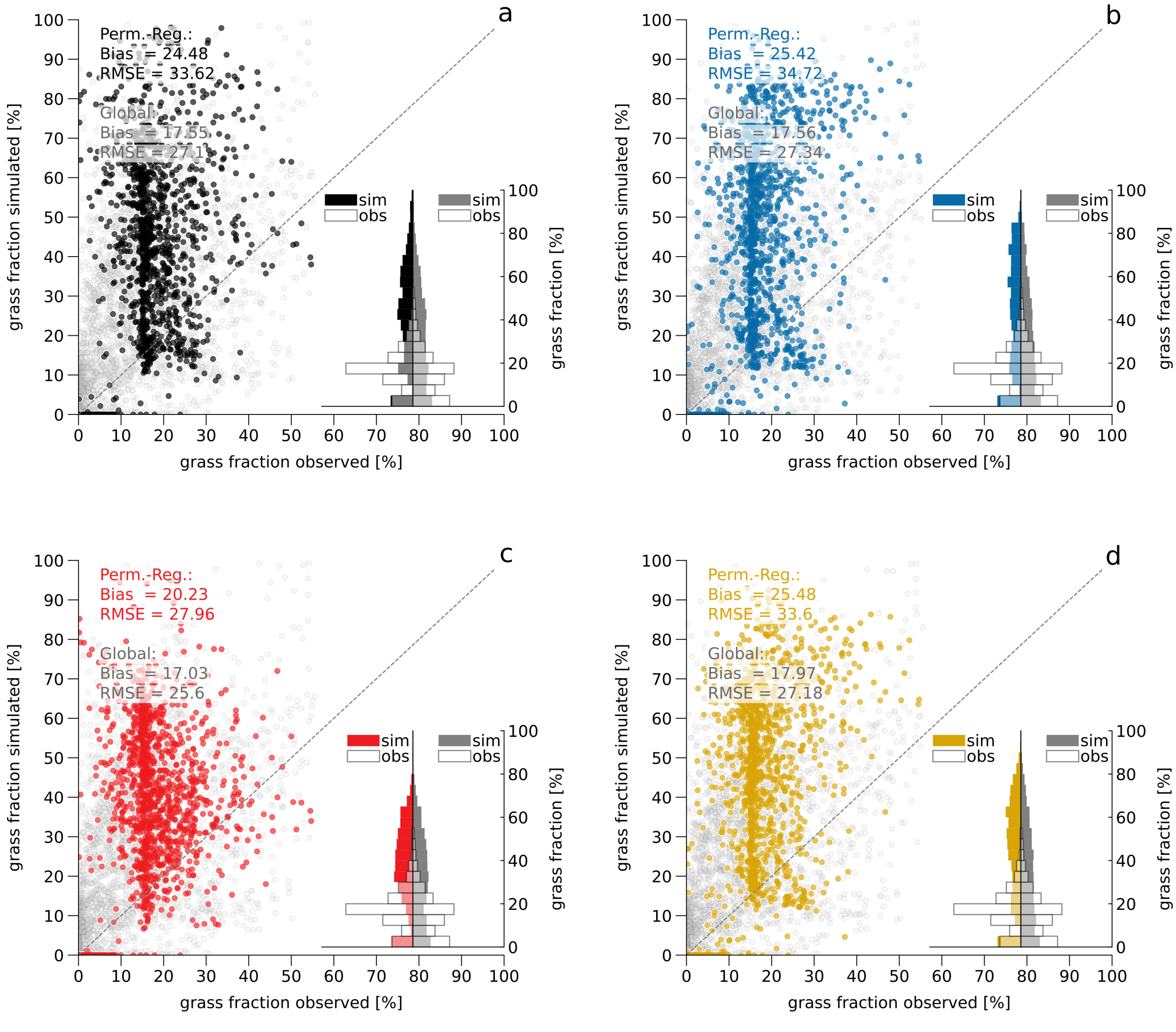

Supplementary Figure SF7. Grass cover fraction

Comparison of simulated and observed (ESA Climate Change Initiative (ESACCI)[69]) average grass cover for: a) MPI-ESM1.2 standard version (black), b) WET setup (blue), c) DRY setup (red) and d) W2D setup (yellow). The data is averaged over the period 1992 - 2020.

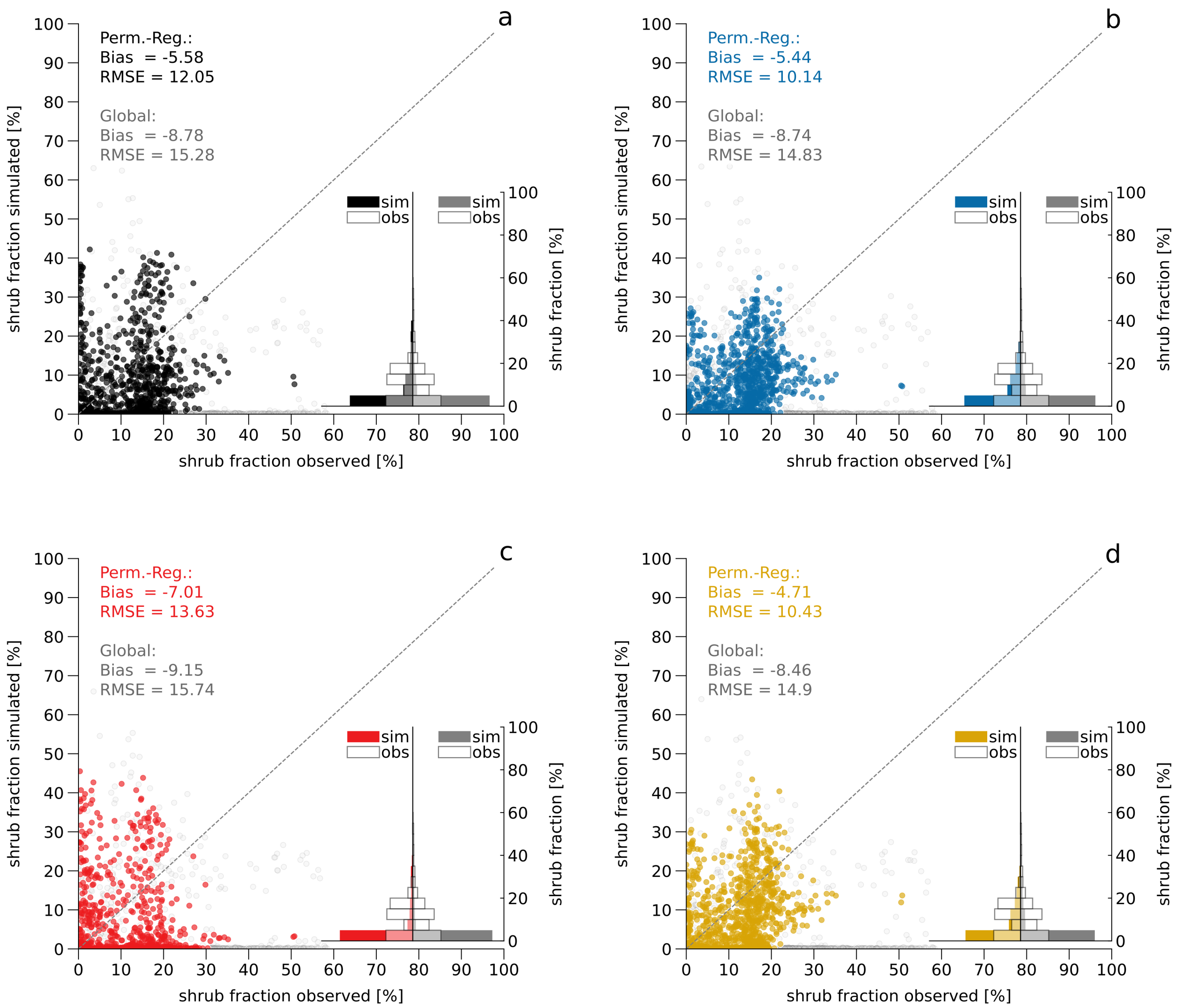

Supplementary Figure SF8. **Shrub cover fraction**

Comparison of simulated and observed (ESA Climate Change Initiative (ESACCI)[69]) average shrub cover for: a) MPI-ESM1.2 standard version (black), b) WET setup (blue), c) DRY setup (red) and d) W2D setup (yellow). The data is averaged over the period 1992 - 2020.

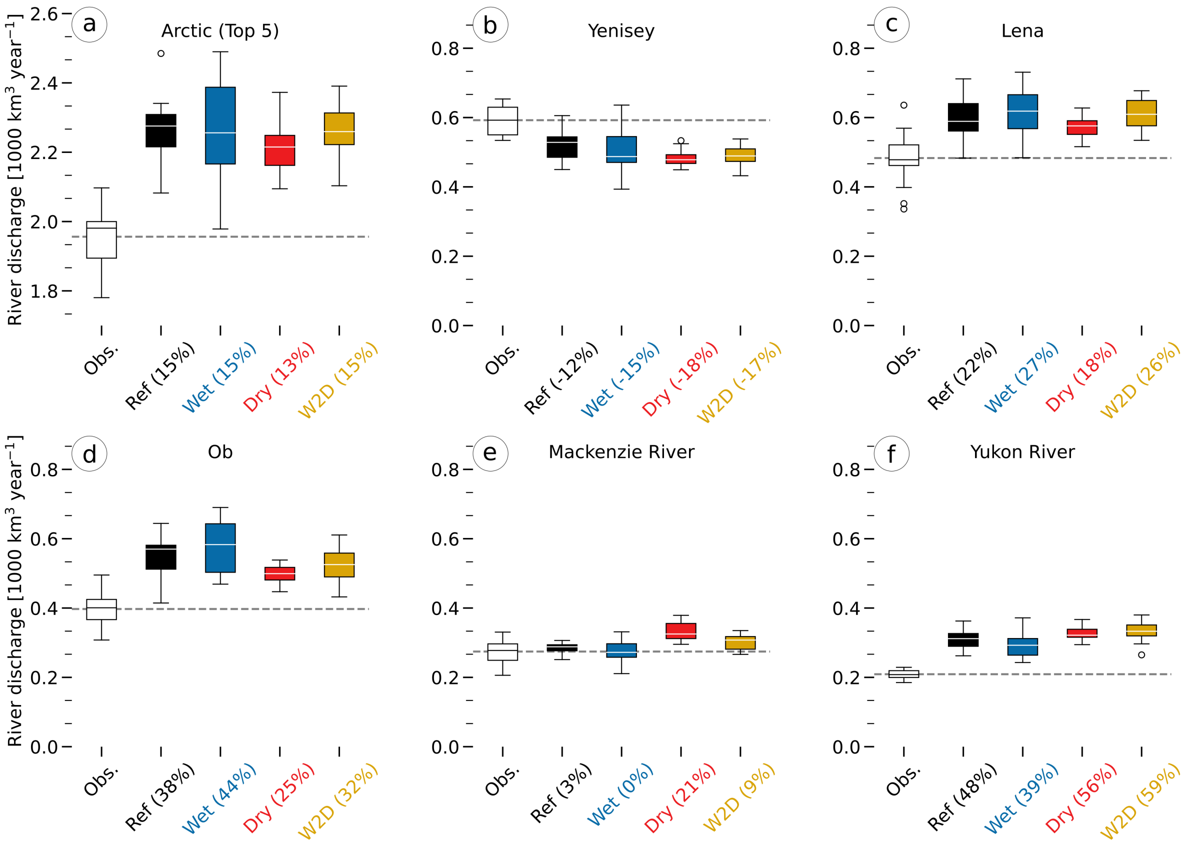

Supplementary Figure SF9. Discharge

Observed (white; Global Runoff Data Centre (GRDC)[68]) and simulated (MPI-ESM1.2 standard version [black], WET setup [blue], DRY setup [red] and W2D setup [yellow]) annual river discharge of: a) the 5 largest Arctic rivers, b) Yenisey, c) Lena d) Ob, e) Mackenzie and f) Yukon. Values in brackets give the relative difference between the simulated and the observed discharge. For each river, the data is averaged over the period with available data between the years 1980 - 1995.

S4 ICON-ESM

The ICON-ESM is the first ESM using the unstructured, icosahedral grid concept of the ICON framework. It consists of the atmospheric component ICON-A, with a non-hydrostatic dynamical core, the ocean model ICON-O, which builds on the same ICON infrastructure but applies the Boussinesq and hydrostatic approximation, and the ICON-L land module. The latter provides a new framework with a flexible scheme of land surface tiling and an object-oriented organization of physical and biogeochemical processes, which allows the coupling of different land surface schemes to the atmospheric and ocean components. For the present investigation we used the land surface model JSBACH4, the sucessor of JSBACH3.2, the land surface component of the latest MPI-ESM version[50]. The model was adapted in the the way as JSBACH3, allowing to simulate dry or wet conditions in the northern permafrost regions. However, as the WEED scheme could not be implemented into JSBACH4 yet, the model does not represent the ponding of water at the land surface and the evapotranspiration from surface water bodies. Furthermore, the natural vegetation dynamics have not yet been enabled in JSBACH4, and neither the changes in plant water availability resulting from the modifications of the permafrost hydrology nor the increase in the atmospheric CO_2 concentrations and in the near-surface temperatures have an effect on the vegetation distribution in the high latitudes. Because of this limited functionality of JSBACH4, we do not include the simulations in the main analysis of this study and merely show the most important results in the supplementary materials (Figs. SF10 - SF12). Overall, the results obtained with ICON-ESM agree well with those of the MPI-ESM simulations, despite ICON-ESM being run at a comparatively low horizontal resolution, i.e. R2B3, in which the globe is resolved by 5120 triangular cells with an average distance between cell centers of 277 km, with the standard 5-layer vertical resolution in land cells, and despite the model simulating a dryer climate in the Acrtic and susbarctic zone.

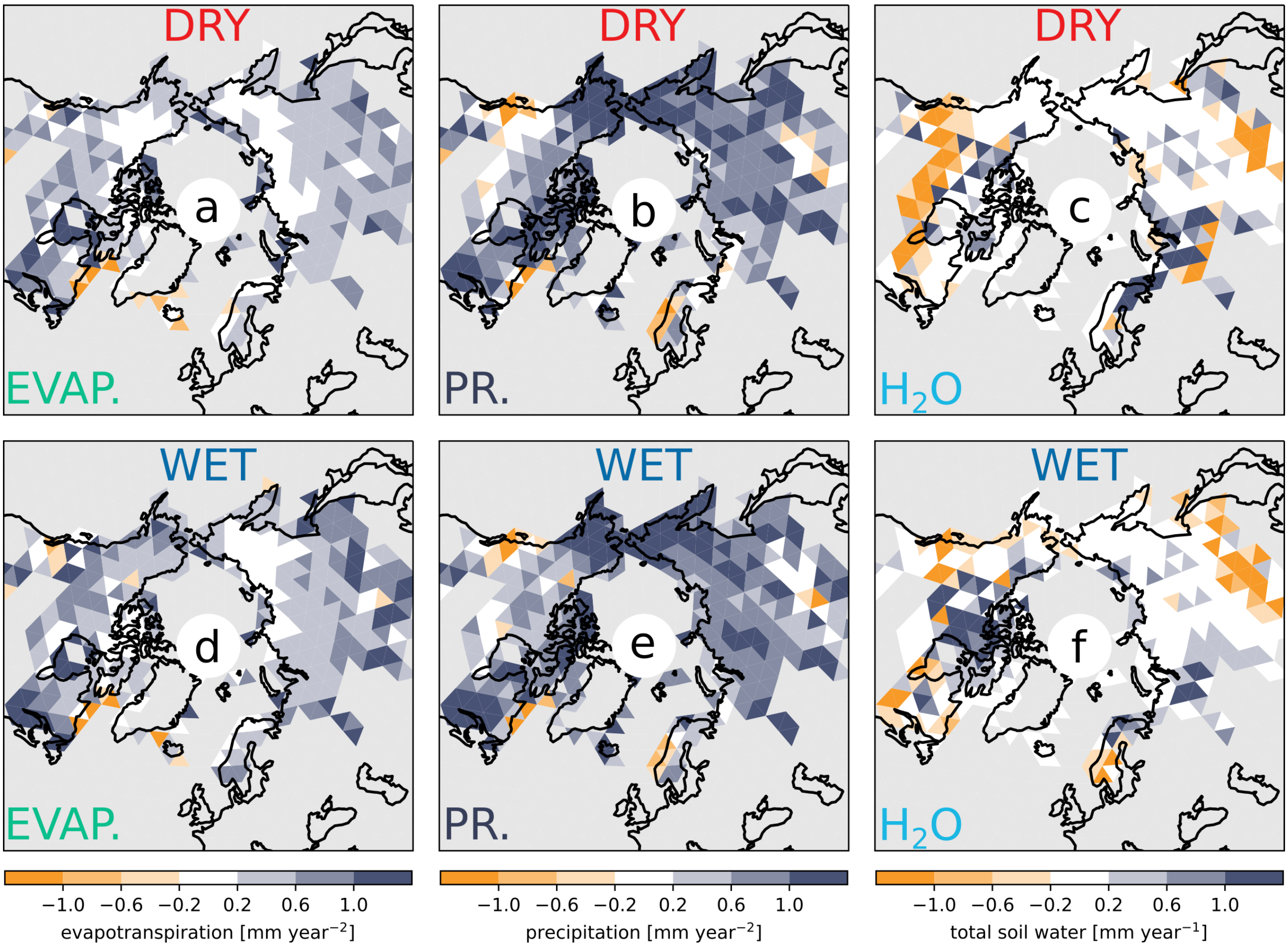

Supplementary Figure SF10. Arctic futures in ICON-ESM
a) 21st century precipitation trend simulated with the DRY ICON-L setup. b) Same as a) but for evapotranspiration. c) Same as a) but for the total soil water (liquid soil moisture and ice) content. d,e,f) Same as a,b,c) but for the WET ICON-L setup. Non-permafrost and glacier grid cells are shaded in grey.

Despite including neither the dynamic vegetation module nor the WEED module and despite being run at a lower resolution, the trends in precipitation and evapotranspiration compare well with the MPI-ESM simulations. However, in contrast to the latter, there are no clear general trends in the total soil water content, either in the DRY or in the WET ICON-L setups. While there are regions that exhibit notable in- and decreases in the total soil water in both simulations, these cancel out on the pan-Arctic scale.

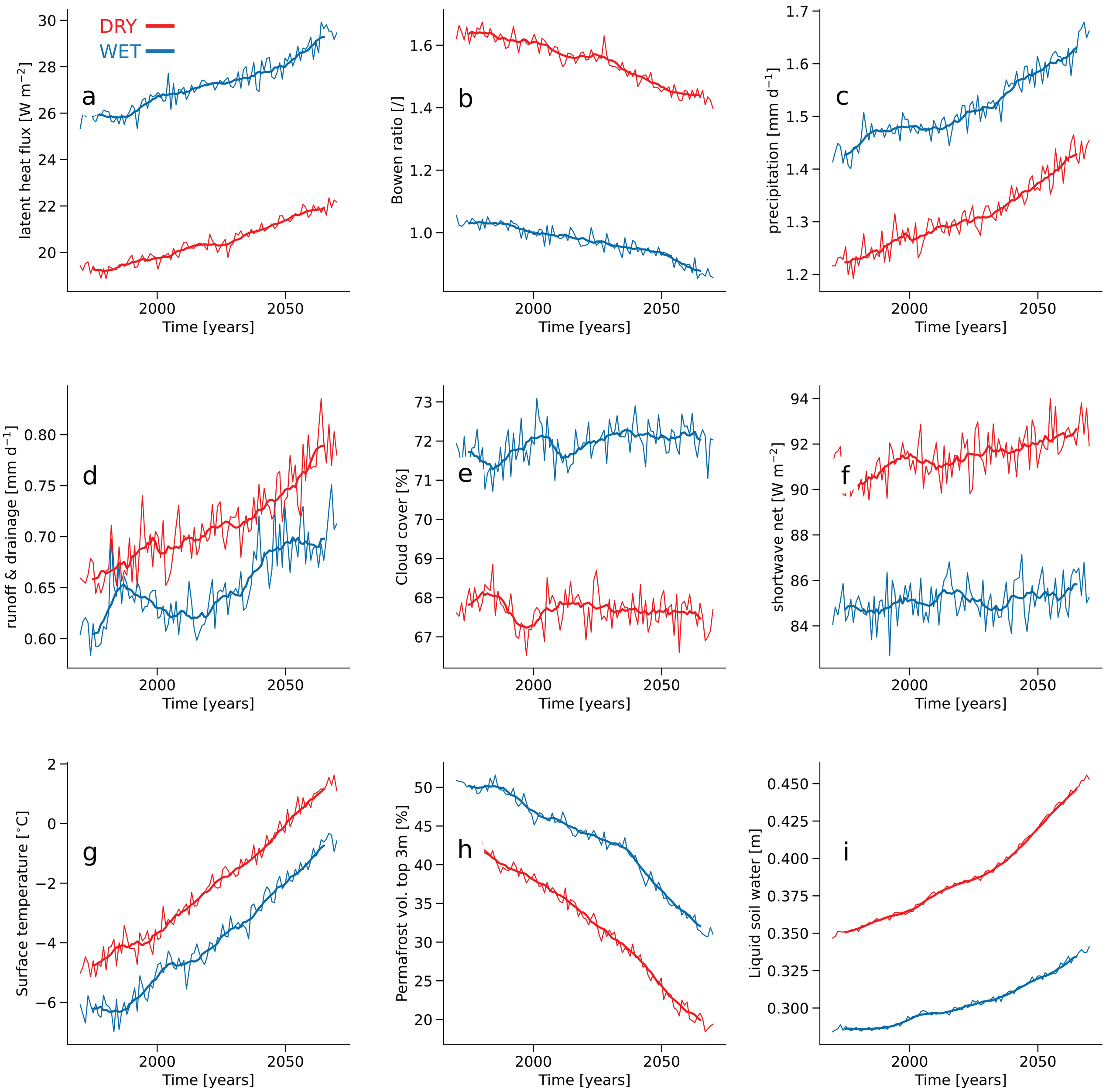

Supplementary Figure SF11. Effects of soil hydrological conditions on near-surface climate:
a) Latent heat flux in the northern permafrost regions in WET (blue) and DRY (red) ICON-ESM simulations for SSP5-8.5. Thin lines show the annual mean, averaged over the northern permafrost regions (note that that grid cells covered by glaciers were excluded), while thick lines give the 10-year running mean. b) Same as a) but showing the Bowen ratio, c) precipitation, d) surface runoff and drainage, e) accumulated cloud cover, f) solar radiation absorbed at the surface, g) surface temperatures, h) near-surface (top 3 m of the soil) permafrost volume and i) liquid soil water content.

The ICON-ESM produces a dryer climate than the MPI-ESM, with a lower cloud cover, less precipitation and, consequently, less evapotraspition, runoff and drainage. Due to the lower cloud cover, the surface shortwave net radiation is also higher, resulting in a higher sensible heat flux and consequently a much higher Bowen ratio. However, despite these differences in climate, the differences between the DRY and WET ICON-L setups generally agree well with those between the WET and DRY MPI-ESM runs.

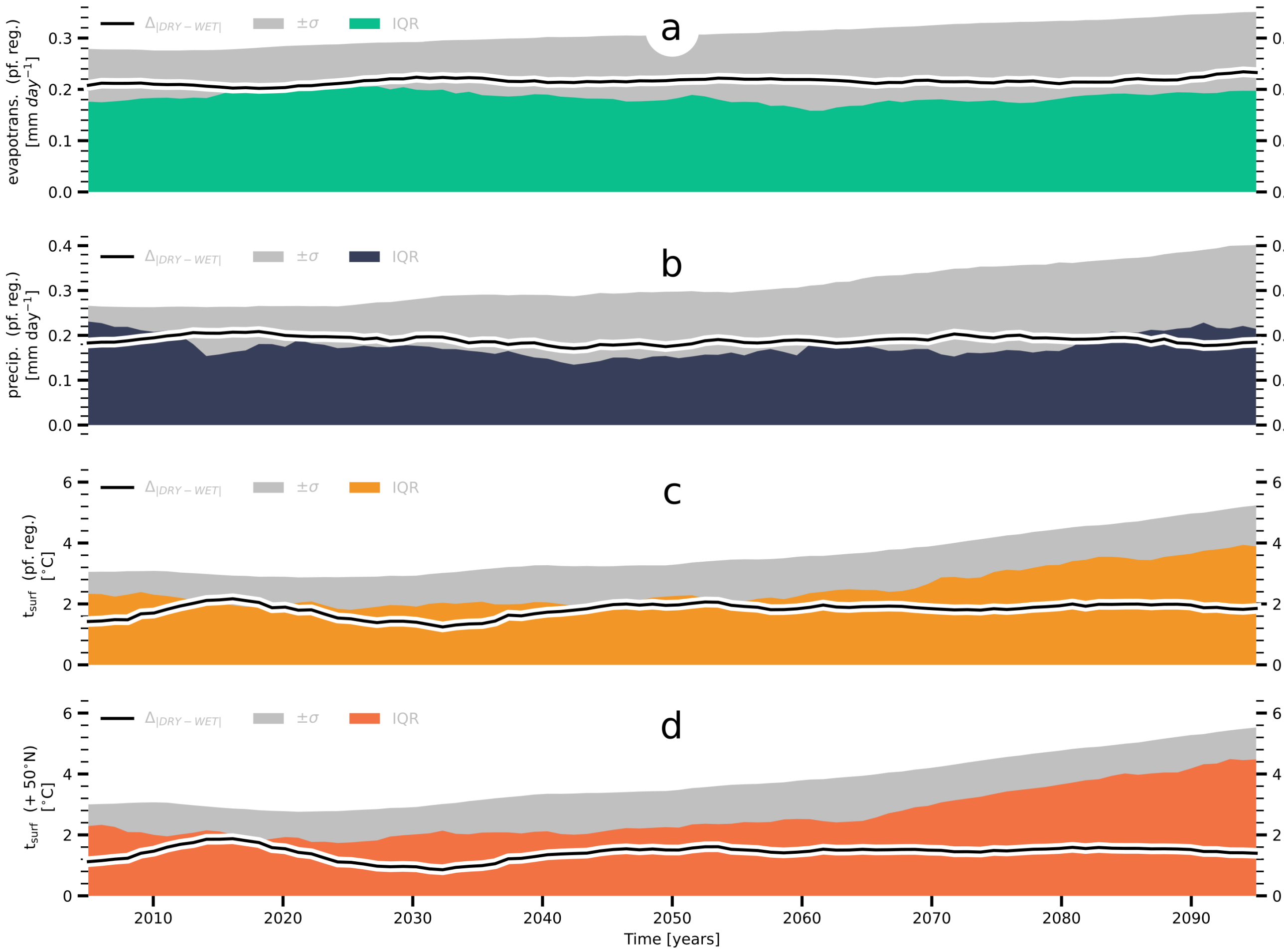

Supplementary Figure SF12. Comparison to CMIP6 ensemble:
a) Differences in evapotranspiration between the WET and the DRY ICON-L setup in permafrost regions ($\Delta^{evap}_{|DRY-WET|}$). Black line gives the interquartile range (IQR^{evap}) — that is the difference between the 75th and the 25th percentile — of the CMIP6 ensemble, while the dotted area provides 2 × the ensemble standard deviation ($\pm\sigma^{evap}$). b) same as a but for precipitation ($\Delta^{pr}_{|DRY-WET|}$, IQR^{pr}, $\pm\sigma^{pr}$), c) surface temperatures in permafrost grid cells ($\Delta^{ts}_{|DRY-WET|}$, IQR^{ts}, $\pm\sigma^{ts}$) and d) surface temperatures (land and ocean) north of 50°N ($\Delta^{ts;+50N}_{|DRY-WET|}$, IQR$^{ts;+50N}$, $\pm\sigma^{ts;+50N}$).

In general, the ICON-ESM simulations agree well with those using the MPI-ESM. However, the differences in the simulated temperatures between the DRY and the WET setups are substantially smaller in the northern permafrost regions (about 0.8°C, which corresponds to about 30 % of the temperature differences in the MPI-ESM simulations) and also those averaged across the latitudes 50°N to 90°N (about 0.6°C, also 30 % of the temperature differences in the MPI-ESM simulations).

Supplementary References

1. Andresen, C. G. *et al.* Soil moisture and hydrology projections of the permafrost region – a model intercomparison. *The Cryosphere* **14**, 445–459 (2020). URL https://doi.org/10.5194/tc-14-445-2020.

2. Telteu, C.-E. *et al.* Understanding each other's models: an introduction and a standard representation of 16 global water models to support intercomparison, improvement, and communication. *Geosci. Model Dev.* **14**, 3843–3878 (2021).

3. Niu, G.-Y., Yang, Z.-L., Dickinson, R. E., Gulden, L. E. & Su, H. Development of a simple groundwater model for use in climate models and evaluation with gravity recovery and climate experiment data. *Journal of Geophysical Research* **112** (2007). URL https://doi.org/10.1029/2006jd007522.

4. Swenson, S. C., Lawrence, D. M. & Lee, H. Improved simulation of the terrestrial hydrological cycle in permafrost regions by the community land model. *Journal of Advances in Modeling Earth Systems* **4**, n/a–n/a (2012). URL https://doi.org/10.1029/2012ms000165.

5. Yang, Z.-L. & Dickinson, R. E. Description of the biosphere-atmosphere transfer scheme (BATS) for the soil moisture workshop and evaluation of its performance. *Global and Planetary Change* **13**, 117–134 (1996). URL https://doi.org/10.1016/0921-8181(95)00041-0.

6. Philip, J. R. EVAPORATION, AND MOISTURE AND HEAT FIELDS IN THE SOIL. *Journal of Meteorology* **14**, 354–366 (1957). URL https://doi.org/10.1175/1520-0469(1957)014<0354:eamahf>2.0.co;2.

7. Beven, K. J. & Kirkby, M. J. A physically based, variable contributing area model of basin hydrology. *Hydrological Sciences Journal* **24**, 43–69 (1979).

8. Gouttevin, I., Krinner, G., Ciais, P., Polcher, J. & Legout, C. Multi-scale validation of a new soil freezing scheme for a land-surface model with physically-based hydrology. *The Cryosphere* **6**, 407–430 (2012). URL https://doi.org/10.5194/tc-6-407-2012.

9. Gerten, D., Schaphoff, S., Haberlandt, U., Lucht, W. & Sitch, S. Terrestrial vegetation and water balance—hydrological evaluation of a dynamic global vegetation model. *Journal of Hydrology* **286**, 249–270 (2004). URL https://doi.org/10.1016/j.jhydrol.2003.09.029.

10. Haxeltine, A. & Prentice, I. C. A general model for the light-use efficiency of primary production. *Functional Ecology* **10**, 551 (1996). URL https://doi.org/10.2307/2390165.

11. Bonan, G. B. Land surface model (lsm version 1.0) for ecological, hydrological, and atmospheric studies: Technical description and users guide. technical note. Tech. Rep., National Center for Atmospheric Research, Boulder, CO (United States ... (1996).

12. Jensen, M. E. & Haise, H. R. Estimating evapotranspiration from solar radiation. *Journal of the Irrigation and Drainage Division* **89**, 15–41 (1963).

13. Thornthwaite, C. W. & Mather, J. R. Instructions and tables for computing potential evapotranspiration and the water balance. Publication 10, 185–311 (Laboratory of Climatology, 1957).

14. Liang, X., Lettenmaier, D. P., Wood, E. F. & Burges, S. J. A simple hydrologically based model of land surface water and energy fluxes for general circulation models. *Journal of Geophysical Research* **99**, 14415 (1994). URL https://doi.org/10.1029/94jd00483.

15. Todini, E. The ARNO rainfall—runoff model. *Journal of Hydrology* **175**, 339–382 (1996). URL https://doi.org/10.1016/s0022-1694(96)80016-3.

16. de Vrese, P., Stacke, T., Kleinen, T. & Brovkin, V. Diverging responses of high-latitude co2 and ch4 emissions in idealized climate change scenarios. *The Cryosphere* **15**, 1097–1130 (2021). URL https://doi.org/10.5194/tc-15-1097-2021.

17. Bi, D. *et al.* Configuration and spin-up of ACCESS-CM2, the new generation australian community climate and earth system simulator coupled model. *Journal of Southern Hemisphere Earth Systems Science* **70**, 225 (2020). URL https://doi.org/10.1071/es19040.

18. Ziehn, T. *et al.* The australian earth system model: ACCESS-ESM1.5. *Journal of Southern Hemisphere Earth Systems Science* **70**, 193 (2020). URL https://doi.org/10.1071/es19035.

19. Semmler, T. *et al.* Simulations for cmip6 with the awi climate model awi-cm-1-1. *Journal of Advances in Modeling Earth Systems* **12**, e2019MS002009 (2020). URL https://agupubs.onlinelibrary.wiley.com/doi/abs/10.1029/2019MS002009. https://agupubs.onlinelibrary.wiley.com/doi/pdf/10.1029/2019MS002009.

20. Wu, T. *et al.* The beijing climate center climate system model (bcc-csm): the main progress from cmip5 to cmip6. *Geoscientific Model Development* **12**, 1573–1600 (2019). URL https://gmd.copernicus.org/articles/12/1573/2019/.

21. Rong, X. *et al.* The CAMS climate system model and a basic evaluation of its climatology and climate variability simulation. *Journal of Meteorological Research* **32**, 839–861 (2018). URL https://doi.org/10.1007/s13351-018-8058-x.

22. Swart, N. C. *et al.* The canadian earth system model version 5 (canesm5.0.3). *Geoscientific Model Development* **12**, 4823–4873 (2019). URL https://gmd.copernicus.org/articles/12/4823/2019/.

23. Danabasoglu, G. *et al.* The community earth system model version 2 (CESM2). *Journal of Advances in Modeling Earth Systems* **12** (2020). URL https://doi.org/10.1029/2019ms001916.

24. Lin, Y. *et al.* Community integrated earth system model (ciesm): Description and evaluation. *Journal of Advances in Modeling Earth Systems* **12**, e2019MS002036 (2020). URL https://agupubs.onlinelibrary.wiley.com/doi/abs/10.1029/2019MS002036. https://agupubs.onlinelibrary.wiley.com/doi/pdf/10.1029/2019MS002036.

25. Cherchi, A. *et al.* Global mean climate and main patterns of variability in the cmcc-cm2 coupled model. *Journal of Advances in Modeling Earth Systems* **11**, 185–209 (2019). URL https://agupubs.onlinelibrary.wiley.com/doi/abs/10.1029/2018MS001369.

26. Roehrig, R. *et al.* The cnrm global atmosphere model arpege-climat 6.3: Description and evaluation. *Journal of Advances in Modeling Earth Systems* **12**, e2020MS002075 (2020). URL https://agupubs.onlinelibrary.wiley.com/doi/abs/10.1029/2020MS002075.

27. Michou, M. *et al.* Present-day and historical aerosol and ozone characteristics in cnrm cmip6 simulations. *Journal of Advances in Modeling Earth Systems* **12**, e2019MS001816 (2020). URL https://agupubs.onlinelibrary.wiley.com/doi/abs/10.1029/2019MS001816.

28. Voldoire, A. *et al.* Evaluation of cmip6 deck experiments with cnrm-cm6-1. *Journal of Advances in Modeling Earth Systems* **11**, 2177–2213 (2019). URL https://agupubs.onlinelibrary.wiley.com/doi/abs/10.1029/2019MS001683.

29. Golaz, J.-C. *et al.* The doe e3sm coupled model version 1: Overview and evaluation at standard resolution. *Journal of Advances in Modeling Earth Systems* **11**, 2089–2129 (2019). URL https://agupubs.onlinelibrary.wiley.com/doi/abs/10.1029/2018MS001603.

30. Burrows, S. M. *et al.* The doe e3sm v1.1 biogeochemistry configuration: Description and simulated ecosystem-climate responses to historical changes in forcing. *Journal of Advances in Modeling Earth Systems* **12**, e2019MS001766 (2020). URL https://agupubs.onlinelibrary.wiley.com/doi/abs/10.1029/2019MS001766.

31. Döscher, R. *et al.* The ec-earth3 earth system model for the climate model intercomparison project 6. *Geoscientific Model Development Discussions* **2021**, 1–90 (2021). URL https://gmd.copernicus.org/preprints/gmd-2020-446/.

32. He, B. *et al.* CAS FGOALS-f3-l model datasets for CMIP6 historical atmospheric model intercomparison project simulation. *Advances in Atmospheric Sciences* **36**, 771–778 (2019). URL https://doi.org/10.1007/s00376-019-9027-8.

33. Li, J. *et al.* Evaluation of famil2 in simulating the climatology and seasonal-to-interannual variability of tropical cyclone characteristics. *Journal of Advances in Modeling Earth Systems* **11**, 1117–1136 (2019). URL https://agupubs.onlinelibrary.wiley.com/doi/abs/10.1029/2018MS001506.

34. Bao, Q. & Li, J. Progress in climate modeling of precipitation over the Tibetan Plateau. *National Science Review* **7**, 486–487 (2020). URL https://doi.org/10.1093/nsr/nwaa006. https://academic.oup.com/nsr/article-pdf/7/3/486/38881335/nwaa006.pdf.

35. Bao, Y., Song, Z. & Qiao, F. Fio-esm version 2.0: Model description and evaluation. *Journal of Geophysical Research: Oceans* **125**, e2019JC016036 (2020). URL https://agupubs.onlinelibrary.wiley.com/doi/abs/10.1029/2019JC016036.

36. Held, I. M. *et al.* Structure and performance of gfdl's cm4.0 climate model. *Journal of Advances in Modeling Earth Systems* **11**, 3691–3727 (2019). URL https://agupubs.onlinelibrary.wiley.com/doi/abs/10.1029/2019MS001829.

37. Dunne, J. P. *et al.* The gfdl earth system model version 4.1 (gfdl-esm 4.1): Overall coupled model description and simulation characteristics. *Journal of Advances in Modeling Earth Systems* **12**, e2019MS002015 (2020). URL https://agupubs.onlinelibrary.wiley.com/doi/abs/10.1029/2019MS002015.

38. Kelley, M. *et al.* Giss-e2.1: Configurations and climatology. *Journal of Advances in Modeling Earth Systems* **12**, e2019MS002025 (2020). URL https://agupubs.onlinelibrary.wiley.com/doi/abs/10.1029/2019MS002025.

39. Miller, R. L. *et al.* Cmip6 historical simulations (1850–2014) with giss-e2.1. *Journal of Advances in Modeling Earth Systems* **13**, e2019MS002034 (2021). URL https://agupubs.onlinelibrary.wiley.com/doi/abs/10.1029/2019MS002034.

40. Swapna, P. *et al.* Long-term climate simulations using the iitm earth system model (iitm-esmv2) with focus on the south asian monsoon. *Journal of Advances in Modeling Earth Systems* **10**, 1127–1149 (2018). URL https://agupubs.onlinelibrary.wiley.com/doi/abs/10.1029/2017MS001262.

41. Volodin, E. M. *et al.* Simulation of the present-day climate with the climate model INMCM5. *Climate Dynamics* **49**, 3715–3734 (2017). URL https://doi.org/10.1007/s00382-017-3539-7.

42. Volodin, E. M. *et al.* Simulation of the modern climate using the inm-cm48 climate model. *Russian Journal of Numerical Analysis and Mathematical Modelling* **33**, 367–374 (2018). URL https://doi.org/10.1515/rnam-2018-0032.

43. Boucher, O. *et al.* Presentation and evaluation of the ipsl-cm6a-lr climate model. *Journal of Advances in Modeling Earth Systems* **12**, e2019MS002010 (2020). URL https://agupubs.onlinelibrary.wiley.com/doi/abs/10.1029/2019MS002010.

44. Hourdin, F. *et al.* Lmdz6a: The atmospheric component of the ipsl climate model with improved and better tuned physics. *Journal of Advances in Modeling Earth Systems* **12**, e2019MS001892 (2020). URL https://agupubs.onlinelibrary.wiley.com/doi/abs/10.1029/2019MS001892.

45. Lurton, T. *et al.* Implementation of the cmip6 forcing data in the ipsl-cm6a-lr model. *Journal of Advances in Modeling Earth Systems* **12**, e2019MS001940 (2020). URL https://agupubs.onlinelibrary.wiley.com/doi/abs/10.1029/2019MS001940.

46. Lee, J. *et al.* Evaluation of the korea meteorological administration advanced community earth-system model (k-ACE). *Asia-Pacific Journal of Atmospheric Sciences* **56**, 381–395 (2019). URL https://doi.org/10.1007/s13143-019-00144-7.

47. Pak, G. *et al.* Korea institute of ocean science and technology earth system model and its simulation characteristics. *Ocean Science Journal* **56**, 18–45 (2021). URL https://doi.org/10.1007/s12601-021-00001-7.

48. Tatebe, H. *et al.* Description and basic evaluation of simulated mean state, internal variability, and climate sensitivity in miroc6. *Geoscientific Model Development* **12**, 2727–2765 (2019). URL https://gmd.copernicus.org/articles/12/2727/2019/.

49. Hajima, T. *et al.* Development of the miroc-es2l earth system model and the evaluation of biogeochemical processes and feedbacks. *Geoscientific Model Development* **13**, 2197–2244 (2020). URL https://gmd.copernicus.org/articles/13/2197/2020/.

50. Mauritsen, T. *et al.* Developments in the mpi-m earth system model version 1.2 (mpi-esm1.2) and its response to increasing co2. *Journal of Advances in Modeling Earth Systems* **11**, 998–1038 (2019). URL https://agupubs.onlinelibrary.wiley.com/doi/abs/10.1029/2018MS001400. https://agupubs.onlinelibrary.wiley.com/doi/pdf/10.1029/2018MS001400.

51. Müller, W. A. *et al.* A higher-resolution version of the max planck institute earth system model (mpi-esm1.2-hr). *Journal of Advances in Modeling Earth Systems* **10**, 1383–1413 (2018). URL https://agupubs.onlinelibrary.wiley.com/doi/abs/10.1029/2017MS001217.

52. Yukimoto, S. *et al.* The meteorological research institute earth system model version 2.0, mri-esm2.0: Description and basic evaluation of the physical component. *Journal of the Meteorological Society of Japan. Ser. II* **97**, 931–965 (2019).

53. Cao, J. *et al.* The nuist earth system model (nesm) version 3: description and preliminary evaluation. *Geoscientific Model Development* **11**, 2975–2993 (2018). URL https://gmd.copernicus.org/articles/11/2975/2018/.

54. Seland, Ø. *et al.* Overview of the norwegian earth system model (NorESM2) and key climate response of CMIP6 DECK, historical, and scenario simulations. *Geoscientific Model Development* **13**, 6165–6200 (2020). URL https://doi.org/10.5194/gmd-13-6165-2020.

55. Tjiputra, J. F. *et al.* Ocean biogeochemistry in the norwegian earth system model version 2 (noresm2). *Geoscientific Model Development* **13**, 2393–2431 (2020). URL https://gmd.copernicus.org/articles/13/2393/2020/.

56. Counillon, F. *et al.* Flow-dependent assimilation of sea surface temperature in isopycnal coordinates with the norwegian climate prediction model. *Tellus A: Dynamic Meteorology and Oceanography* **68**, 32437 (2016). URL https://doi.org/10.3402/tellusa.v68.32437.

57. Lee, W.-L. *et al.* Taiwan earth system model version 1: description and evaluation of mean state. *Geoscientific Model Development* **13**, 3887–3904 (2020). URL https://gmd.copernicus.org/articles/13/3887/2020/.

58. Sellar, A. A. *et al.* Ukesm1: Description and evaluation of the u.k. earth system model. *Journal of Advances in Modeling Earth Systems* **11**, 4513–4558 (2019). URL https://agupubs.onlinelibrary.wiley.com/doi/abs/10.1029/2019MS001739.

59. Kuhlbrodt, T. *et al.* The low-resolution version of hadgem3 gc3.1: Development and evaluation for global climate. *Journal of Advances in Modeling Earth Systems* **10**, 2865–2888 (2018). URL https://agupubs.onlinelibrary.wiley.com/doi/abs/10.1029/2018MS001370.

60. Williams, K. D. *et al.* The met office global coupled model 3.0 and 3.1 (gc3.0 and gc3.1) configurations. *Journal of Advances in Modeling Earth Systems* **10**, 357–380 (2018). URL https://agupubs.onlinelibrary.wiley.com/doi/abs/10.1002/2017MS001115.

61. Dirmeyer, P. A. *et al.* GSWP-2: Multimodel analysis and implications for our perception of the land surface. *Bull. Am. Meteorol. Soc.* **87**, 1381–1398 (2006).

62. Kim, H. Global soil wetness project phase 3 atmospheric boundary conditions (experiment 1) (2017).

63. Christiansen, H. H. *et al.* The thermal state of permafrost in the nordic area during the international polar year 2007-2009. *Permafrost and Periglacial Processes* **21**, 156–181 (2010). URL https://doi.org/10.1002/ppp.687.

64. Romanovsky, V. E., Smith, S. L. & Christiansen, H. H. Permafrost thermal state in the polar northern hemisphere during the international polar year 2007-2009: a synthesis. *Permafrost and Periglacial Processes* **21**, 106–116 (2010). URL https://doi.org/10.1002/ppp.689.

65. Smith, S. *et al.* Thermal state of permafrost in north america: a contribution to the international polar year. *Permafrost and Periglacial Processes* **21**, 117–135 (2010). URL https://doi.org/10.1002/ppp.690.

66. Brown, J., Hinkel, K. M. & Nelson, F. E. The circumpolar active layer monitoring (calm) program: Research designs and initial results1. *Polar Geography* **24**, 166–258 (2000). URL https://doi.org/10.1080/10889370009377698.

67. Brown, R. D. & Brasnett, B. Canadian meteorological centre (cmc) daily snow depth analysis data, version 1., cmc_swe_mly_clim_1998to2012_v01.2. NASA National Snow and Ice Data Center Distributed Active Archive Center, Boulder, Colorado USA (2010). URL https://nsidc.org/data/NSIDC-0447/versions/1. Accessed: 06.03.2021.

68. Grdc: Long-term statistics and annual characteristics of grdc timeseries data. Online provided by the Global Runoff Data Centre of WMO. Koblenz: Federal Institute of Hydrology (BfG) (2021). URL https://www.bafg.de/GRDC/EN/02_srvcs/21_tmsrs/210_prtl/prtl_node.html.

69. Georgievski, G. & Hagemann, S. Characterizing uncertainties in the ESA-CCI land cover map of the epoch 2010 and their impacts on MPI-ESM climate simulations. *Theor. Appl. Climatol.* **137**, 1587–1603 (2019).